PCCP

Highly sensitive gating in pH-responsive nanochannels as a result of ionic bridging and nanoconfinement

Journal:	*Physical Chemistry Chemical Physics*
Manuscript ID	CP-ART-03-2018-002028.R1
Article Type:	Paper
Date Submitted by the Author:	12-May-2018
Complete List of Authors:	Lopez, Luis; Northwestern University Department of Biomedical Engineering, Nap, Rikkert; Northwestern University, Department of Biomedical Engineering

Journal Name

ARTICLE

Highly sensitive gating in pH-responsive nanochannels as a result of ionic bridging and nanoconfinement

Luis G. Lopez*[a] and Rikkert J. Nap[a]

Received 00th January 20xx,
Accepted 00th January 20xx

DOI: 10.1039/x0xx00000x

www.rsc.org/

Sensitive switching between OFF and ON states is a desirable feature in stimuli-responsive nanopores and nanochannels. In this work, we show that nanogates modified with weak polyelectrolytes can be controlled by multivalent counterions and, more remarkably, can exhibit sensitive pH-gating due to an interplay between ionic bridging and nanoconfinement. We demonstrate these general features by systematically studying the effects of Ca^{2+} binding on the molecular organization and transport properties of poly(acrylic acid)-functionalized nanochannels. To this end, we extend and apply a molecular theory that has been successfully used in the past to describe and predict the behavior of pH-responsive polymers. Two main results emerge from the present study: First, the addition of Ca^{2+} to the bulk solution changes—in a concentration-dependent manner—both the ionization and structural state of the end-tethered polymers, affecting, respectively, the ionic conductivity and physical opening of the nanochannel. Second, in the presence of Ca^{2+} and under specific nanoconfinement conditions, the grafted channel can exhibit a sensitive response to pH in the transition between closed and open states. We attribute this sensitivity to bistability in the system. Our results also indicate that the polymer layer can undergo a microphase separation when the brush collapses on the nanochannel walls. Taken together, these findings suggest the possibility of designing nanogates that can respond to marginal changes in pH or multivalent ion concentration. Such nanodevices may be used as logic gates or for any application that requires a sensitive control over the ions, molecules, or nanoparticles flowing through them.

Introduction

Smart nanopores and nanochannels[1-5] are designed nanoscale devices with transport properties that can be controlled by external stimuli, such as light,[6, 7] temperature,[8, 9] pH,[10, 11] ions,[12, 13] molecules,[14, 15] or some combination thereof.[16] These nanodevices can be opened or closed to the passage of ions, molecules, macromolecules, or even nanoparticles,[17] by applying or removing the gating stimulus. The broad spectrum of stimuli that can be used, as well as the diversity of species that can be selectively transported, make these nanogates adaptable to a wide variety of needs. Among many potential applications, stimuli-responsive nanopores (which have a length, L, comparable to the radius, R) and nanochannels ($R << L$) can be used as (macro)molecular sieves, water transporters, ion detectors, and ionic gates.[3, 18] The design of these nanodevices is generally inspired by observing biological systems such as the nuclear pore complex,[19] ion channels,[20] and ion pumps.[21, 22] In addition to their biomimetic properties, synthetic artificial systems can have some advantages over their natural counterparts. For example, solid-state nanochannels can be more durable and mechanically robust than lipid-embedded channels.[3] Similar to biological systems, the diversity of these artificial bioinspired nanodevices seems to have no limits.

Among a wide variety of designs, the category constituted by nanochannels modified with end-tethered weak polyelectrolytes has received considerable attention during the last few years.[10, 23-31] These channels are characterized by their pH-gating properties, which result from the pH-responsive nature of the polymer, and exhibit a non-trivial coupling between charge transport and molecular organization.[24] When a weak polyelectrolyte-modified nanochannel is used as an ionic gate, one of the most important quantities to be measured is its conductivity, which can be controlled by the local proton concentration.[10] Two general types of ionic gates can be constructed depending on the nature of the weak polyelectrolyte used to modified the channel, namely, polybase or polyacid chains.

As previous research has shown,[27-29, 32, 33] a poly(acrylic acid) (PAA) nanogate is conductive at pH values above the apparent pK_a of the polymers end-tethered to the inner surface of the channel, and non-conductive at lower pH. In the conductive state the polymers are swollen and negatively charged, while in the non-conductive state they are "coiled" and neutral. Although the cited studies have described the relationship between pH-responsiveness and conductivity, they were all conducted in the absence of crosslinking ions (*i.e.*, counterions

[a] Department of Biomedical Engineering, Department of Chemistry and Chemistry of Life Processes Institute, Northwestern University, Evanston, Illinois 60208, United States. E-mail: luis.lopez@northwestern.edu

†Electronic Supplementary Information (ESI) available: Detailed description of the free energy functional terms. Minimization of the free energy functional. Molecular details. Determination of the dissociation constant values for AH, ANa, ACa^+, and A_2Ca. Effect of changing the electrolyte solution (from NaCl to KCl) on the conductance of the nanochannel. Variation of the electrostatic potential within the channel. Effects of the grafting density and C_{NaCl} on the conductance of the channel and thickness of the end-tethered PAA layer. Interplay between polymer density and calcium binding. Discontinuity in the nanochannel conductance. See DOI: 10.1039/x0xx00000x

that interact strongly with the charged polymer segments and form bridges between them). From the study of polyelectrolytes end-tethered to planar[34, 35] and spherical[36] surfaces, it is known that multivalent ions can neutralize and shrink the oppositely charged polymer layer. It has been shown that, in general, anionic polyelectrolyte layers exhibit a higher selectivity for cations of higher valence.[34, 37] For planar end-tethered PAA layers in the salted regime, it has been experimentally observed that monovalent counterions like sodium or cesium cause chain stretching, while divalent ions like Ca^{2+} induce polymer collapse.[38] We expected, then, that the use of divalent crosslinking ions, like Ca^{2+}, would have a significant effect on both the conductivity and opening of the channel to the passage of molecular cargo through it.

Thus, the purpose of this paper is to study the effects of Ca^{2+} binding and nanoconfinement on the pH-gating properties of nanochannels modified with poly(acrylic acid). To this end, we extended and applied a molecular theory that has been successfully used in the past to describe the molecular behavior of a poly(4-vinylpyridine) (P4VP)-modified nanochannel and correctly predict its experimentally measured conductance.[23] The theoretical approach described by Tagliazucchi *et al.*[23] was combined with a molecular theory recently developed to study the effects of divalent ion binding on PAA-coated nanoparticles.[39]

The resulting molecular theory predicts that calcium ions can neutralize and crosslink the negatively charged PAA chains. Our results show how this property can be used to control the nanochannel conductance as well as the transport of molecules or nanoparticles through it. In addition, the theory describes how cylindrical nanoconfinement due to the channel geometry allows the end-tethered layer to exhibit two kinds of ionic crosslinked states, one with the polymers collapsed on the channel walls, and one with the polymers condensed toward the center of the channel. The former corresponds to a structurally open state and the latter to a closed one. More remarkably, the theory predicts that, under specific conditions, both states are almost equally stable. We show that this property, which is completely absent in planar and spherical end-tethered polymer layers, enables the system to respond with great sensitivity to changes in pH or Ca^{2+} concentration. Finally, our theoretical calculations indicate that a microphase separation can take place in the system when the polymers collapse on the nanochannel walls. In summary, our results reveal the importance of studying the effects of different crosslinking ions (or mixtures of them) on end-tethered weak polyelectrolytes under nanoconfinement and provide guidelines for the design of bioinspired artificial nanopores and nanochannels with sensitive gating properties.

Theoretical approach

The aim of the theory applied here is to describe the behavior of a single nanochannel modified with a monodisperse end-tethered layer of poly(acrylic acid) chains, in the presence of calcium ions (Figure 1). The system under study consisted of N_P chains end-tethered to the inner surface of a cylindrical nanochannel of radius R and internal area $A(R)$. The grafting density or surface coverage is defined by $\sigma = N_P/A(R)$. The PAA chains have a degree of polymerization of N, and each acrylic acid segment can be in one of five states; namely, protonated (AH), deprotonated (A^-), sodium-bound (ANa), or calcium-bound (either as ACa^+ or as part of a calcium bridge, *i.e.*, an A_2Ca complex). Thus, the theory allows for the system to have charge regulation, a mechanism that controls the net charge of the confined polymers depending on the structure of the end-tethered layer as well as the distribution and local density of free charges. In other words, the system can reduce the local electrostatic repulsions by shifting the acid-base equilibrium toward uncharged segments or by forming counter ion-condensed states. Therefore, the resulting state of the monomers, *i.e.*, the number of (de)protonated and condensed states, is not imposed, but results from the minimization of the free energy. Importantly, the resulting ionization state of the polymer under confinement will be different from its expected state in free solution. This feature was found to be essential to predict, both qualitatively and quantitatively, the experimental conductance of a P4VP-modified nanochannel,[23] and likewise essential to accurately predict the thickness of PAA grafted to planar layers.[40] Another remarkable feature of our theoretical approach is the absence of adjustable parameters.

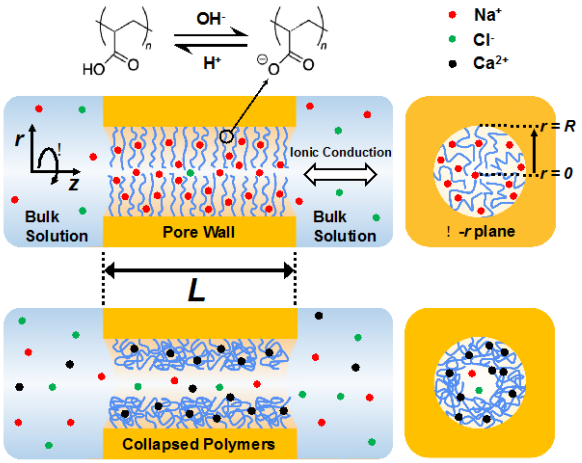

Figure 1. Schematic representation of a poly(acrylic) acid-functionalized nanogate, at basic pH, with (top) and without (bottom) calcium ions in the bulk solution. R is the radius and L is the length of the cylindrical pore (channel). While nanopores have a length comparable to the radius, the lengths of nanochannels are much larger than their radii ($R << L$). Ionic currents can be induced by applying an electric potential difference across the nanogate (aspect not studied in this work).

Following previous treatments,[23, 41] one starts by writing down the free energy as a functional of (1) the probability distribution function corresponding to the polymer conformations; (2) the number densities of all free species; and (3) the different interaction fields. These functions are position-dependent. The present approach assumes inhomogeneity only in the radial direction (r). The expression for the total free energy, F, includes the following contributions

$$\mathrm{F} = -TS_{conf} - TS_{trans} + F_{chem} + F_{elect} + E_{vdW} + E_{rep} \quad (1)$$

where T is the temperature, S_{conf} is the conformational entropy of the end-tethered polymer chains; S_{trans} represents the translational entropy corresponding to all free species (Na^+, Cl^-, Ca^{2+}, H^+, OH^-, and water); F_{chem} is the free energy associated with the set of chemical equilibria (Table 1); F_{elect} corresponds to the total electrostatic energy; E_{vdW} models the effective van der Waals (vdW) attractions between segments; and E_{rep} represents the steric repulsions between the molecular species. The formal definition and detailed description of each term of eq. 1, as well as its minimization, are given in the ESI†.

Table 1. Dissociation constants* for carboxylic acid monomers.

reaction	*pK$_d$*
$AH \rightleftharpoons A^- + H^+$	*5.0*
$ANa \rightleftharpoons A^- + Na^+$	*-0.40*
$ACa^+ \rightleftharpoons A^- + Ca^{2+}$	*1.0*
$A_2Ca \rightleftharpoons 2A^- + Ca^{2+}$	*4.0*

* Values based on experimental data and molecular dynamics simulations (for more details, see ESI†).

The ionization state and conductance of the nanochannel as well as its structural state are quantified by using the following definitions. The mean dissociation fraction of PAA segments can be calculated as

$$\langle f_i \rangle = \frac{\int_0^R G(r) f_i(r) \langle \phi_P(r) \rangle \, dr}{\int_0^R G(r) \langle \phi_P(r) \rangle \, dr} \quad (2)$$

where $\langle \phi_p(r) \rangle$ is the polymer volume fraction and $G(r)$ is a geometrical factor (see ESI†). The average ion concentration within the channel is determined from the equation

$$\langle c_i \rangle = \frac{2}{R^2} \int_0^R c_i(r) r \, dr \quad (3)$$

where $c_i(r)$ is the molar concentration of the species i at r.

The ionic conductance of the nanochannel, G, can be estimated using the Nernst-Plank equation under the Goldman constant field approximation.[42-44] This approach has been successfully applied in the past to predict the experimentally measured conductance of a P4VP-functionalized nanochannel.[23] Under these approximations, which assume quasi-equilibrium conditions (*i.e.*, currents tending to zero), the total conductance of the channel is equal to the sum of the conductance due to each free ion inside the nanochannel (Na^+, Cl^-, Ca^{2+}, OH^-, H^+). Correspondingly, the conductance contribution of each mobile ionic species is calculated using its diffusion coefficient, D_i, as well as its average concentration inside the channel, as predicted by the molecular theory under zero applied potential. The resulting expression, assuming one-dimensional diffusion along the z axis and equilibrium conditions at the nanochannel inlets, is given by

$$\mathrm{G} = \frac{I}{V} = \frac{2\pi F^2}{LRT} \sum_{i=k} q_i^2 D_i \int_0^R c_i(r) r \, dr \quad (4)$$

where the index k runs over all the free ions inside the nanochannel (Na^+, Cl^-, Ca^{2+}, OH^-, H^+). Although our molecular theory is formulated for a channel of infinite length, the conductance of a channel of finite length can be calculated, as long as $R \ll L$. The nanochannel dimensions used for the conductance calculations (R = 7.5 nm and L = 12 μm) are within the ranges where these approximations have been validated; namely, channel radii larger than two Debye lengths[45-47] and channel lengths greater than 100 nm.[44] Moreover, since we are considering a channel length on the micrometer order, the polarization contributions at the nanochannel inlets can be neglected without losing essential information.[44] This expression assumes that (1) bound counterions (Ca^{2+} and Na^+) do not contribute to the conductance of the system, in other words, there is no fast exchange between bound and free ions; and (2) the diffusion coefficients are those of the bulk solution and are not affected by the polymer density.

In order to quantify the thickness or height of the end-tethered PAA layer, h, we took twice the first moment (mean value) of the polymer volume fraction distribution, as follows

$$h = \frac{2 \int_0^R G(r) \langle \phi_P(r) \rangle (R - r) \, dr}{\int_0^R G(r) \langle \phi_P(r) \rangle \, dr} \quad (5)$$

where the factor of 2 and the radius, R, are applied so that, in the limit of low curvature, this height definition reduces to the conventional height used for planar end-tethered layers.

Results and discussion

All results presented in this paper were obtained for a channel of radius R = 7.5 nm (Figure 1). Unless otherwise specified, we also used a fixed value for the NaCl concentration in the bulk solution (C_{NaCl} = 0.15 M). The effects of changing C_{NaCl}, as well as the grafting density, are shown in the ESI†.

Effects of calcium binding on the nanochannel conductance. The state of protonation/deprotonation and the apparent pK_a of the chargeable groups of a weak polyelectrolyte depend on many factors besides pH, including chain length, local polymer density and ionic concentration, as well as the geometry of the system. For instance, it has been demonstrated that, due to the mentioned factors, the apparent pK_a values found in planar[48-50] and cylindrical[41] end-tethered weak polyelectrolyte layers differ from those in the bulk solution. In addition, a significant shift in the apparent pK_a of the basic groups of P4VP chains due to the curvature of the channel has been reported for P4VP-modified nanochannels.[23] In this context, the property of charge

regulation (see Theoretical approach section) has been shown to be essential to describe the pH-responsiveness of a weak polyelectrolyte-modified nanochannel and to predict its conductance. In this work, we go further and examine the effects of a multivalent ion (Ca^{2+}) on the nanochannel conductance.

The effects of calcium binding on the ionic properties of a PAA-modified nanochannel can be better appreciated by analyzing the system at the extremes of a calcium concentration range (Figure 2). At a negligible Ca^{2+} concentration in the bulk solution ($C_{Ca}^{2+} = 10^{-7}$ M), our theoretical calculations show how the carboxylic acid groups of PAA are gradually deprotonated as the pH increases (see the upper plot of Figure 2a).

It is important to stress that the amount of charged monomers, in the PAA layer, is much lower than might have been expected based upon the pH of the solution, due to the phenomenon of charge regulation. Namely, as the acid groups get deprotonated they experience unfavorable electrostatic interactions, which are reduced by (i) chain stretching, resulting in a loss of conformational entropy, (ii) counterion confinement, at the cost of translational entropy, (iii) charge regulation, by shifting the chemical equilibrium to its protonated state, at the cost of chemical free energy, and (iv) counterion condensation of sodium and calcium ions. Thus, the degree of deprotonation and structure of the PAA layer results from a balance between electrostatic interactions, entropic forces, exclude volume repulsions, ion condensation, and acid-base equilibrium.

As deprotonation occurs, the negatively charged polymers recruit counterions from the bulk reservoirs, mainly sodium ions in this case. Due to the relatively weak association between each carboxylate group and Na^+ (see Table 1), only a fraction of the deprotonated segments is neutralized by sodium cations. At the same time, through electrostatic interactions, the remaining negatively charged segments keep (without binding) a significant number of free sodium cations inside the nanochannel, while expelling ions of the same charge as the polymer—in this case Cl^- (Figure 2a, middle plot). In agreement with the report of Tagliazucchi *et al.*,[23] these results show the high degree of ion selectivity that such a polymer grafted nanodevice can exhibit, and how the nanoconfined environment can become a "unipolar solution" of counterions.[51] More importantly, the large concentration of the majority charge carrier within the channel (Na^+), which in turn depends on the amount of deprotonated polymer segments, controls the nanochannel conductance, *G* (Figure 2a, lower panel).

Calcium ions exhibit strong, specific interactions with COO^- groups and can form bridges between them (Table 1). Thus, we expected that increasing the concentration of calcium ions in the bulk solution would dramatically change the ionization and structural state of a PAA-modified nanochannel and, consequently, its transport properties. There are several enthalpic and entropic contributions influencing the formation of calcium bridges between negatively charged polymer segments. Carboxylate groups bind Ca^{2+} much more strongly than Na^+, especially when an A_2Ca complex is formed (Table 1). Due to its divalent nature, Ca^{2+} can form stable bridges between COO^- groups belonging to the same or to a different polymer chain. The energetically favorable ionic bridging collapses the polymer layer[39] (see next section), even though this implies a reduction in the conformational entropy of the polymers. Simultaneously, due to ionic crosslinking, the number of charged polymer segments drops, reducing the electrostatic repulsions between polymer chains. Ionic bridging also increases the translational entropy of ions, since fewer counterions need to be confined within the polymer layer. Finally, the osmotic pressure of the system decreases by exchanging two bound Na^+ by one bound Ca^{2+}.

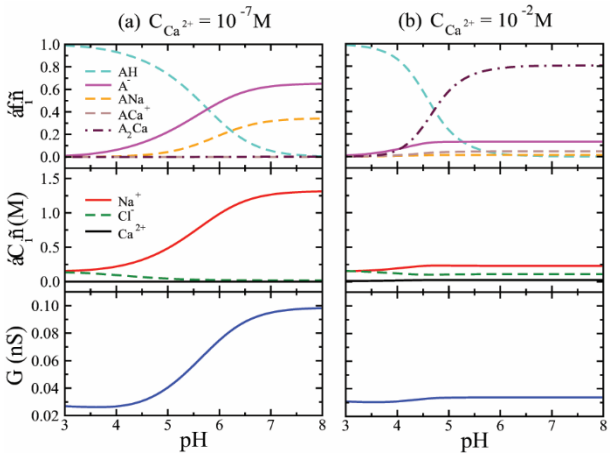

Figure 2. From top to bottom, the pH dependence of: the average fraction of PAA segment states, $\langle f_i \rangle$; the average concentration of salt ions inside the channel, $\langle C_i \rangle$; and the nanochannel conductance, *G*. The parameters used for these calculations were: $N = 45$, $\sigma = 0.1$ chains/nm^2, and $C_{NaCl} = 0.15$ M. Calculations were made at different calcium concentrations: (a) $C_{Ca}^{2+} = 10^{-7}$ M and (b) $C_{Ca}^{2+} = 10^{-2}$ M. The conductance was calculated for a channel of radius $R = 7.5$ nm and length $L = 12$ μm. Nanochannels with these dimensions have been previously studied, both experimentally[10] and theoretically.[23] The effects of using KCl instead of NaCl, as the electrolyte solution, are considered in the ESI (see Figure S1 and S2).

The molecular theory applied here accounts for all these contributions. It explains the changes observed in the ionization state of the polymers, as a function of pH, in the presence of 10^{-2} M of Ca^{2+} in the bulk solution (Figures 2a,b upper plots). Namely, the promotion of deprotonation of the carboxylic groups, the extinction of the ANa complexes, and the absolute predominance of A_2Ca bridges over ACa^+ complexes. This last feature should be emphasized, since it shows that the formation of calcium bridges is entirely responsible for the neutralization of the charged brush.

For the particular case examined in Figure 2b ($C_{Ca}^{2+} = 10^{-2}$ M), the neutralization of the polymers is not total; a significant fraction of deprotonated segments (greater than 10%) remains in the end-tethered layer. The presence of these charged groups produces a minor uptake of Na^+ and its associated electrostatic

potential is not significant enough for the complete expulsion of Cl^-, as shown in the middle plot of Figure 2b. Thus, sodium and chloride ions inside the channel are the charge carriers that sustain the residual conductance observed in the lower plot of Figure 2b. The negligible amount of free Ca^{2+} inside the channel shows that almost all calcium ions are bound to carboxylate groups. These results illustrate that the degree of deprotonation of the polymers, which is responsible for the recruitment of counterions, can be significantly lowered by the addition of calcium ions, concomitantly causing a dramatic drop in nanochannel conductance.

Figure 3 shows how conductance changes between the two extreme cases presented in Figures 2a,b. These results reveal that calcium concentration, together with pH, can be used to regulate nanochannel conductance. As Figure 3 shows, neutralization of the carboxylate groups by calcium ions is as effective as the protonation of these groups in reducing the conductance of the channel. The dependence of conductance on the grafting density as well as the bulk NaCl concentration are presented in Figures S3 and S4, respectively.

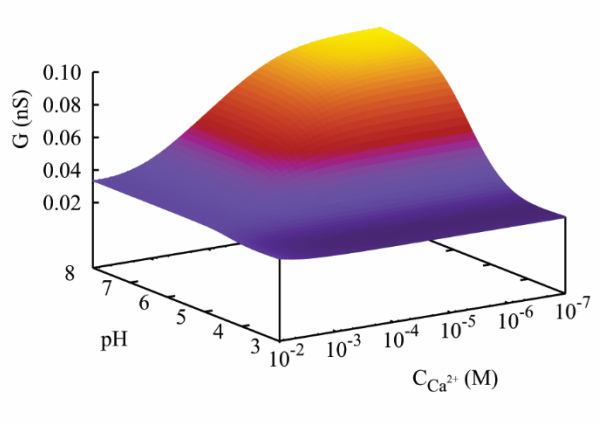

Figure 3. Conductance landscape as a function of both pH and calcium concentration, $C_{Ca^{2+}}$. The parameters used are the same as in Figure 2: N = 45, σ = 0.1 chains/nm^2, C_{NaCl} = 0.15 M, R = 7.5 and L = 12 μm.

Control of the nanochannel opening by calcium ions. The binding of calcium ions to the charged groups of PAA can not only affect the conductivity of the channel but can also collapse the end-tethered PAA chains. This alteration, in turn, can have a direct effect on the opening of the channel. In order to evince this property, we set the pH at 8 (the highest pH value considered in this study) and compared the state of the polymers in the absence and presence of Ca^{2+} (Figure 4). It can be clearly seen that the molecular organization of the nanochannel (extended versus collapsed polymers) is highly dependent on the presence of calcium ions. Calcium is able to dramatically collapse the negatively charged end-tethered layer through the same enthalpic and entropic contributions explained in the previous section. Since we assume good-solvent conditions, the formation of stable inter- and intramolecular bridges (A_2Ca) is the only factor driving the observed polymer shrinking.

Observe that figure 4 displays the polymer volume fraction as function of position in the channel, whereas Figure 2 shows the spatial average of the ion concentrations and polymer chemical states. Other spatial dependent quantities, like the electrostatic potential (see Figure S5), follow a behavior similar to that of the polymer volume fraction shown in Figure 4. At high pH and zero or low calcium concentrations, the charged PAA layer fills the channel almost uniformly. Consequently, the electrostatic potential is flat but no zero, resulting in an increase in sodium and a decrease in chloride ion concentrations and a large conductance as shown in Figure 2 and 3. For calcium concentrations in the range of 0.1-10 mM, the PAA layer collapses and is neutralized due to calcium bridge formation. The polymer density and electrostatic potential reduces to zero at the center of the channel, while within the collapsed layer a small electrostatic potential remains, due to residual deprotonated PAA monomers. The potential within the layer reduces further as calcium concentration is increased. The results shown in Figure 4 and S5 emphasize the interplay between structural organization and physical interactions and its effect on functional properties.

In order to examine the opening state of the channel for a wider set of conditions, the thickness of the polymer layer, h, was plotted as a function of pH and calcium concentration. This dependence, for a specific case of a nanochannel functionalized with PAA chains of 45 segments, is depicted in Figure 5. The plot shows that calcium concentrations above 10^{-3} M and pH values above 5 are necessary to induce a significant collapse of the polymers. The results also show that the transition between collapsed and extended states occurs as smoothly as pH and calcium concentration are varied. The effects of changing the grafting density and C_{NaCl} on the layer thickness are presented in Figures S6 and S7, respectively.

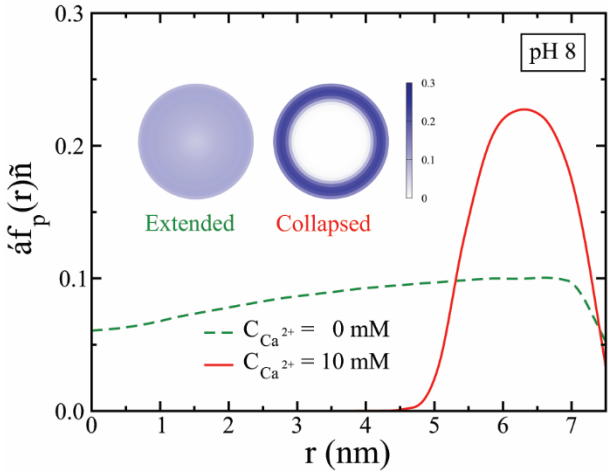

Figure 4. Polymer volume fraction, $\langle\phi_P(r)\rangle$, as a function of the distance, r, from the center of the channel (0 nm) to the wall (7.5 nm). The values of the parameters are the same as for Figure 2 and 3, but here the system has a fixed bulk pH of 8, to highlight the effect

of calcium ions. The green/dashed (red/solid) curve corresponds to the polymer distribution in the absence (presence) of calcium ions. The inset shows the cross-sectional polymer volume fraction, $\langle \phi_p(r) \rangle$, of the nanochannel for both states.

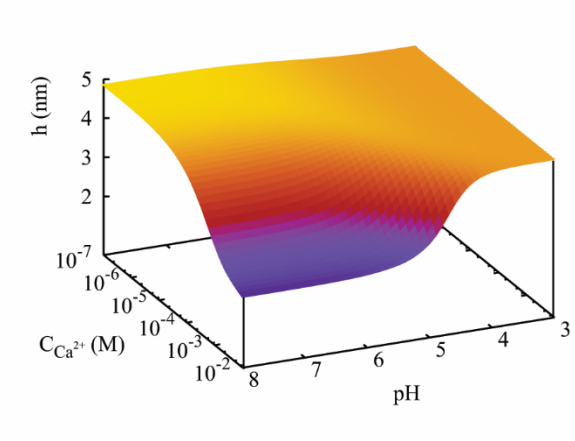

Figure 5. End-tethered polymer layer thickness, h, as a function of pH and calcium concentration, $C_{Ca}{}^{2+}$. The number of segments, N, and polymer density, σ, used here are the same as in Figures 2-4 (N = 45 and σ = 0.1 chains/nm^2).

The regulation of PAA thickness by calcium ions has direct implications for controlling the passage of nanoparticles/molecules through PAA-functionalized nanogates. In the extended state (with on average swollen and negatively charged polymers), the nanochannel is conductive but structurally closed. In other words, the extended polymers act as a physical barrier, blocking the passage of molecular cargo through the channel. In the collapsed state, the nanochannel is non-conductive, but is open enough to allow large cargo to enter and flow through it.

Sensitive response of the nanochannel in the presence of Ca^{2+}. Given a fixed polymer grafting density, σ, nanoconfinement can be increased either by decreasing the nanochannel radius or by increasing the polymer length. The result of these changes is a higher polymer density toward the center of the channel. We report the results of keeping the value of the radius constant (R = 7.5 nm) and varying the number of segments per polymer chain. This allowed the study of the effects of polymer density on the organization of the polymers inside the nanochannel, in the presence of calcium ions (C_{Ca2+} = 10^{-2} M). Depending on the chain length, three structural behaviors are observed (Figure 6).

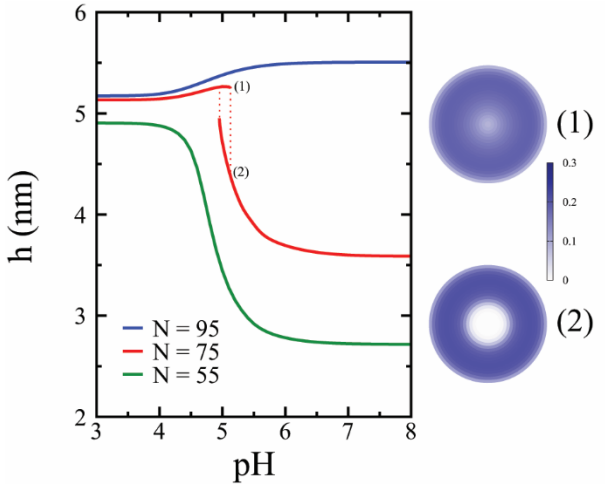

Figure 6. Left: pH dependence of the layer thickness, h, for different polymer lengths; N is the number of polymer segments for each case. The calculations were made for a fixed polymer density of σ = 0.1 chains/nm^2, C_{NaCl} = 0.15 M, and $C_{Ca}{}^{2+}$ = 10^{-2} M. Right: Corresponding cross sections of the nanochannel (with N = 75) at pH 5.1, showing both the center-phase (1) and the wall-phase (2).

For short polymer lengths, an increase in pH produces a smooth transition from the extended state to the collapsed state. In this case, polymer condensation induced by calcium ions occurs toward the channel walls, as seen in Figure 4. In contrast, for longer chains, polymer condensation occurs toward the central axis of the channel. In addition, continuous chain stretching is observed as the pH is increased. This type of condensation happens when the number of calcium bridges at the center of the channel is high enough to partially compensate for the entropic cost of stretched chain conformations.

However, the most remarkable structural behavior is found for intermediate-length chains, where a discontinuous response is observed (Figure 6). For these chain lengths, the end-tethered layer shows a highly sensitive response to pH. In other words, the channel can be physically open or closed within a narrow pH window. This behavior may be attributed to the existence of stable and metastable states within the window of pH values where the jumps occur. Bistable collective behavior was previously reported for a coarse-grained model of neutral polymers end-grafted within a cylinder.[52] In that work, the authors showed that the relative stability of wall and center phases depends on both the range and strength of attractive interactions between polymer segments. For the system considered in this paper, calcium bridging is the only factor mediating the attraction between polymer segments. This suggests that the number of calcium bridges could be different depending on whether the polymers are collapsed on the walls or condensed toward the center of the channel.

In order to examine this interpretation, in the context of the bistable behavior found near $\sigma \sim$ 0.1 chains/nm^2 (Figure 6), we plotted the average fraction of the different acidic group states as a function of the grafting density (Figure S8a). The plot clearly

shows that the fraction of calcium bridges (A_2Ca complexes) displays different dependencies on polymer density when the polymer condensation takes place on the walls (grafting densities less than 0.1 chains/nm^2) or toward the center of the channel (grafting densities greater than 0.1 chains/nm^2). In addition, Figure S8b shows that this behavior disappears for a lower calcium concentration. In this case, the fraction of A_2Ca complexes increases monotonically with the grafting density, without any discontinuity. Therefore, these results indicate that the jump found for intermediate lengths, in the presence of 10^{-2} M Ca^{2+}, reflects two different behaviors that result from the interplay between calcium bridging and the polymer density inside the channel. Due to this feature, calcium ions can induce a highly sensitive switch in the state of the pore/channel.

Regarding the conductivity of the channel, a discontinuous change was also observed under the same conditions as specified for Figure 6, as described in Figure S9 and the corresponding discussion in the ESI†. We believe that the bistable behavior found for intermediate length chains can be used in the design of nanogates where a sensitive control of the ions, (macro)molecules, or nanoparticles flowing through them is desirable.

Microphase separation induced by Ca^{2+}. Under certain conditions, polymer brushes can phase separate into lateral inhomogeneous domains. However, since tethered polymers lack translation mobility, the phase separation does not result in macroscopically separated phases. Instead, laterally inhomogeneous microscopic-sized domains or patterns, such as stripes or micelles, occur.[53] It has recently been reported that trivalent ions are able to induce lateral structural inhomogeneities and drive phase separation in planar polyelectrolyte brushes through ionic bridging.[54] Although similar research has not been done for calcium ions and poly(acrylic acid) brushes, there are reasons to expect the formation of microphase separated domains induced by calcium bridging in PAA-modified nanochannels. First, as shown in the present work for nanochannels, and in a very recent paper for planar layers and coated nanoparticles,[39] calcium ions are able to collapse end-tethered PAA layers through ionic bridging. Second, as work on PAA-coated nanoparticles has shown,[39] the curvature of the grafted surface strongly influences the collapse induced by calcium ions. Hence, the negative curvature of the channel walls could facilitate the formation of lateral inhomogeneities. Since our theoretical approach allows inhomogeneity only in the radial direction, r (Figure 1), we cannot directly observe the formation of any lateral arrangement by looking at the cross-sectional polymer volume fraction of the nanochannel. However, instabilities present in the system, which may indicate microphase separation, can be revealed by examining thermodynamic quantities such as the chemical potential of the polymers, $\mu_p = \partial W/\partial N_p$ (where N_p is the number of grafted chains), and lateral pressure, $\Pi_a = \partial W/\partial A$.[55]

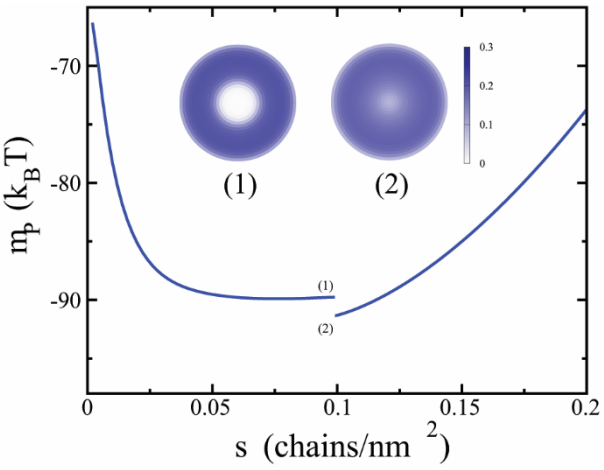

Figure 7. Chemical potential of the polymer chains, μ_P, vs. grafting density, σ, for a polymer length of N = 75, at pH 5.1 and $C_{Ca}^{2+} = 10^{-2}$ M. The sodium chloride concentration in the bulk solution is the same as in Figures 2–6 (C_{NaCl} = 0.15 M). The nanochannel cross sections shown as inset plots, (1) and (2), correspond to a grafting density of 0.0991 chains/nm^2 and 0.0992 chains/nm^2, respectively.

To this end, we examined the case of a nanochannel modified with chains of 75 segments (same conditions as in Figure 6) and plotted the polymer chemical potential as a function of grafting density, σ (Figure 7). Two distinctive features can be observed in the chemical potential curve. First, the existence of two branches separated by a discontinuity near σ = 0.1 chains/nm^2, precisely the grafting density in Figure 6. It is important to note here that the left branch of the curve ($\sigma <$ 0.1 chains/nm^2) corresponds to wall-phase configurations, while the right branch ($\sigma >$ 0.1 chains/nm^2) corresponds to center-phase configurations. Second, the presence of a negative slope in the left branch of the curve. This feature indicates an unstable homogeneous system for the wall-phase configurations, indicating the presence of microphase-separated structures induced by calcium ions.

In order to complement the calculated results for polymer chemical potential, we looked at the behavior of the pressure-area isotherms,[55] *i.e.*, Π_a versus $1/\sigma$, for different calcium ion concentrations. As Figure 8 shows, at relatively low Ca^{2+} concentrations, the lateral pressure is positive for all values of area per chain and increases monotonically as the area per chain is reduced. In other words, the repulsive forces within the layer increase monotonically as the system become denser, behavior expected for partially charged polymers, indicating that the homogeneous system is stable. In contrast, the curve is non-monotonic for a calcium concentration of 10^{-2} M. The lateral pressure goes to zero for an infinite value of $1/\sigma$, but becomes negative as the area per chain is reduced. As in the case of the corresponding chemical potential curve, there is a discontinuity at the 'minimum' of the lateral pressure curve, reflecting the existence of wall-phase and center-phase configurations. The negative compressibility, exhibited when the area per chain is higher than ~10 nm^2/chain (wall-phase

configurations), is consistent, again, with microphase separation induced by calcium ions.

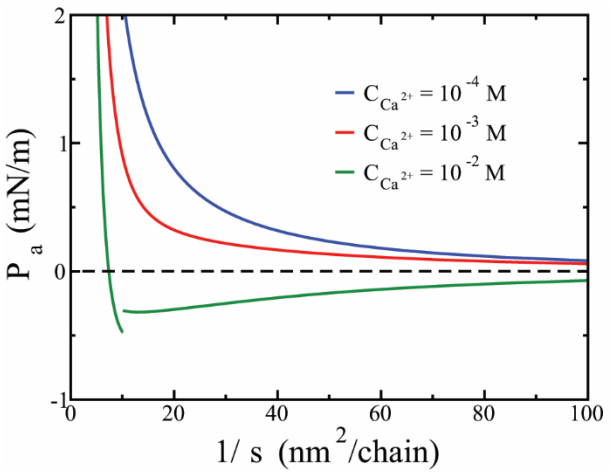

Figure 8. Lateral pressure, Π_a, as a function of the area per polymer chain, $1/\sigma$, for different calcium concentrations. The parameters used for these calculations were: N = 75, pH 5.1, and C_{NaCl} = 0.15 M.

Conclusions

On the basis of a molecular theory, we systematically investigated the effects of calcium binding on the structural and functional properties of PAA-functionalized nanochannels. We found that (1) the addition of calcium ions to the bulk solution dramatically changes both the ionization state and the molecular organization of the nanochannel, which can be used to control, respectively, the conductivity of the channel and the transport of molecular cargo through it; (2) in the presence of calcium ions and under specific nanoconfinement conditions, the nanochannel exhibits a sensitive response to pH and calcium concentration, which can be attributed to bistable behavior in the system; (3) a microphase separation induced by calcium ions, and probably facilitated by the curvature of the channel, may occur when the polymers collapse on the walls of the channel.

Our findings may be instructive for future theoretical and experimental studies on weak polyelectrolyte modified nanogates, as well as for the design of related nanodevices, particularly when sensitive gating is required. In addition, our results suggest that the use of other multivalent counterions may expand the spectrum of behaviors as well as the regulatory properties of nanogates functionalized with polyelectrolytes, substantially broadening the potential applications of these nanodevices.

Conflicts of interest

There are no conflicts to declare.

Acknowledgements

Research supported as part of the Center for Bio-Inspired Energy Science, an Energy Frontier Research Center funded by the U.S. Department of Energy (DOE), Office of Science, Basic Energy Sciences (BES), under Award # DE-SC0000989. The authors thank Prof. Igal Szleifer and Dr. Mario Tagliazucchi for useful discussions.

REFERENCES

1. X. Hou, W. Guo and L. Jiang, *Chemical Society Reviews*, 2011, **40**, 2385-2401.
2. M. Tagliazucchi and I. Szleifer, *Materials Today*, 2015, **18**, 131-142.
3. K. Xiao, L. Wen and L. Jiang, *Small*, 2016, **12**, 2810-2831.
4. Z. Zhang, X. Sui, P. Li, G. Xie, X.-Y. Kong, K. Xiao, L. Gao, L. Wen and L. Jiang, *Journal of the American Chemical Society*, 2017, **139**, 8905-8914.
5. Z. Zhang, L. Wen and L. Jiang, *Chemical Society Reviews*, 2018, **47**, 322-356.
6. A. Brunsen, J. Cui, M. Ceolín, A. D. Campo, G. J. A. A. Soler-Illia and O. Azzaroni, *Chemical Communications*, 2012, **48**, 1422-1424.
7. K. Xiao, X. Y. Kong, Z. Zhang, G. Xie, L. Wen and L. Jiang, *Journal of Photochemistry and Photobiology C: Photochemistry Reviews*, 2016, **26**, 31-47.
8. B. Yameen, M. Ali, R. Neumann, W. Ensinger, W. Knoll and O. Azzaroni, *Small*, 2009, **5**, 1287-1291.
9. W. Guo, H. Xia, F. Xia, X. Hou, L. Cao, L. Wang, J. Xue, G. Zhang, Y. Song, D. Zhu, Y. Wang and L. Jiang, *ChemPhysChem*, 2010, **11**, 859-864.
10. B. Yameen, M. Ali, R. Neumann, W. Ensinger, W. Knoll and O. Azzaroni, *Nano Letters*, 2009, **9**, 2788-2793.
11. M. Ali, S. Nasir, P. Ramirez, J. Cervera, S. Mafe and W. Ensinger, *ACS Nano*, 2012, **6**, 9247-9257.
12. Y. Tian, X. Hou, L. Wen, W. Guo, Y. Song, H. Sun, Y. Wang, L. Jiang and D. Zhu, *Chemical Communications*, 2010, **46**, 1682-1684.
13. L. Gao, P. Li, Y. Zhang, K. Xiao, J. Ma, G. Xie, G. Hou, Z. Zhang, L. Wen and L. Jiang, *Small*, 2015, **11**, 543-547.
14. Z. Sun, C. Han, L. Wen, D. Tian, H. Li and L. Jiang, *Chemical Communications*, 2012, **48**, 3282-3284.
15. Y. Jiang, N. Liu, W. Guo, F. Xia and L. Jiang, *Journal of the American Chemical Society*, 2012, **134**, 15395-15401.
16. Y. B. Zheng, S. Zhao, S. H. Cao, S. L. Cai, X. H. Cai and Y. Q. Li, *Nanoscale*, 2017, **9**, 433-439.
17. S. Tan, L. Wang, H. Liu, H. Wu and Q. Liu, *Nanoscale Research Letters*, 2016, **11**, 50.
18. H. Zhang, Y. Tian and L. Jiang, *Nano Today*, 2016, **11**, 61-81.
19. F. Alber, S. Dokudovskaya, L. M. Veenhoff, W. Zhang, J. Kipper, D. Devos, A. Suprapto, O. Karni-Schmidt, R. Williams, B. T. Chait, A. Sali and M. P. Rout, *Nature*, 2007, **450**, 695-701.
20. Y. Kurachi and A. North, *The Journal of Physiology*, 2004, **554**, 245-247.
21. E. Gouaux and R. MacKinnon, *Science*, 2005, **310**, 1461-1465.
22. D. C. Gadsby, *Nature Reviews Molecular Cell Biology*, 2009, **10**, 344-352.
23. M. Tagliazucchi, O. Azzaroni and I. Szleifer, *Journal of the American Chemical Society*, 2010, **132**, 12404-12411.
24. M. Tagliazucchi, Y. Rabin and I. Szleifer, *Journal of the American Chemical Society*, 2011, **133**, 17753-17763.

25. M. Tagliazucchi and I. Szleifer, *Soft Matter*, 2012, **8**, 7292-7305.
26. M. Tagliazucchi, Y. Rabin and I. Szleifer, *ACS Nano*, 2013, **7**, 9085-9097.
27. H. Zhang, X. Hou, L. Zeng, F. Yang, L. Li, D. Yan, Y. Tian and L. Jiang, *Journal of the American Chemical Society*, 2013, **135**, 16102-16110.
28. H. Zhang, X. Hou, J. Hou, L. Zeng, Y. Tian, L. Li and L. Jiang, *Advanced Functional Materials*, 2015, **25**, 1102-1110.
29. H. Zhang, Y. Tian, J. Hou, X. Hou, G. Hou, R. Ou, H. Wang and L. Jiang, *ACS Nano*, 2015, **9**, 12264-12273.
30. G. Chen and S. Das, *Journal of Physical Chemistry B*, 2016, **120**, 6848-6857.
31. C. Zhou, L. Mei, Y. S. Su, L. H. Yeh, X. Zhang and S. Qian, *Sensors and Actuators, B: Chemical*, 2016, **229**, 305-314.
32. X. Hou, H. Zhang and L. Jiang, *Angewandte Chemie - International Edition*, 2012, **51**, 5296-5307.
33. J. Wu, N. Wang, H. Zhang, L. Wang, H. Dong, Y. Zhao and L. Jiang, *Journal of Materials Chemistry A*, 2013, **1**, 4642-4646.
34. J. Yu, J. Mao, G. Yuan, S. Satija, Z. Jiang, W. Chen and M. Tirrell, *Macromolecules*, 2016, **49**, 5609-5617.
35. J. Yu, J. Mao, G. Yuan, S. Satija, W. Chen and M. Tirrell, *Polymer*, 2016.
36. A. Ezhova and K. Huber, *Macromolecules*, 2016, **49**, 7460-7468.
37. J. Karppi, S. Åkerman, K. Åkerman, A. Sundell and I. Penttilä, *Journal of Polymer Research*, 2010, **17**, 71-76.
38. O. Borozenko, C. Ou, W. G. Skene and S. Giasson, *Polymer Chemistry*, 2014, **5**, 2242-2252.
39. R. J. Nap, S. H. Park and I. Szleifer, *Soft Matter*, 2018, **14**, 2365-2378.
40. P. Gong, T. Wu, J. Genzer and I. Szleifer, *Macromolecules*, 2007, **40**, 8765-8773.
41. R. Nap, P. Gong and I. Szleifer, *Journal of Polymer Science, Part B: Polymer Physics*, 2006, **44**, 2638-2662.
42. D. E. Goldman, *J. Gen. Physiol.*, 1943, **27**, 37-60.
43. P. Ramírez, S. Mafé, A. Alcaraz and J. Cervera, *Journal of Physical Chemistry B*, 2003, **107**, 13178-13187.
44. I. Vlassiouk, S. Smirnov and Z. Siwyt, *Nano Letters*, 2008, **8**, 1978-1985.
45. B. Corry, S. Kuyucak and S. H. Chung, *Biophysical Journal*, 2000, **78**, 2364-2381.
46. B. Corry, S. Kuyucak and S. H. Chung, *Chemical Physics Letters*, 2000, **320**, 35-41.
47. G. Moy, B. Corry, S. Kuyucak and S. H. Chung, *Biophysical Journal*, 2000, **78**, 2349-2363.
48. R. Israels, A. M. Leermakers, G. J. Fleer and E. B. Zhulina, *Macromolecules*, 1994, **27**, 3249-3261.
49. P. Gong, J. Genzer and I. Szleifer, *Physical Review Letters*, 2007, **98**.
50. R. Dong, M. Lindau and C. K. Ober, *Langmuir*, 2009, **25**, 4774-4779.
51. H. Daiguji, P. Yang and A. Majumdar, *Nano Letters*, 2004, **4**, 137-142.
52. D. Osmanovic, J. Bailey, A. H. Harker, A. Fassati, B. W. Hoogenboom and I. J. Ford, *Physical Review E - Statistical, Nonlinear, and Soft Matter Physics*, 2012, **85**.
53. O. Peleg, M. Tagliazucchi, M. Kröger, Y. Rabin and I. Szleifer, *ACS Nano*, 2011, **5**, 4737-4747.
54. J. Yu, N. E. Jackson, X. Xu, B. K. Brettmann, M. Ruths, J. J. de Pablo and M. Tirrell, *Science Advances*, 2017, **3**.
55. M. A. Carignano and I. Szleifer, *The Journal of Chemical Physics*, 1994, **100**, 3210-3223.